Materials Research
Express

INCLUSIVE PUBLISHING
TRUSTED SCIENCE

PURPOSE-LED
PUBLISHING™

PAPER • **OPEN ACCESS**

Sputtering power-driven structural and bonding evolution in vanadium-doped diamond-like carbon films

To cite this article: Görkem Yumuşak and Bahadır Tunaboylu 2026 *Mater. Res. Express* **13** 116401

View the article online for updates and enhancements.

You may also like

- Energetics of carbon and nitrogen impurities and their interactions with vacancy in vanadium
Juan Hua, , Yue-Lin Liu et al.
- Synthesis and elastic properties of V_2AlC thin films by magnetron sputtering from elemental targets
Darwin P Sigumonrong, Jie Zhang, Yanchun Zhou et al.
- Phase equilibria, phases and compounds in the V–C system
Vladimir N Lipatnikov

This content was downloaded from IP address 31.223.97.178 on 10/06/2026 at 06:59

Materials Research Express

Check for updates

OPEN ACCESS

RECEIVED
13 March 2026

REVISED
9 April 2026

ACCEPTED FOR PUBLICATION
2 June 2026

PUBLISHED
10 June 2026

Original content from this work may be used under the terms of the Creative Commons Attribution 4.0 licence.

Any further distribution of this work must maintain attribution to the author(s) and the title of the work, journal citation and DOI.

PAPER

Sputtering power-driven structural and bonding evolution in vanadium-doped diamond-like carbon films

Görkem Yumuşak* and **Bahadır Tunaboylu**

Department of Metallurgical and Materials Engineering, Marmara University, Istanbul, Türkiye

* Author to whom any correspondence should be addressed.

E-mail: gorkem.yumusak@marmara.edu.tr

Keywords: diamond-like carbon (DLC), vanadium doping, XPS, chemical bonding, vanadium carbide (VC), magnetron sputtering

Abstract

Vanadium-doped diamond-like carbon (V-DLC) films were deposited on silicon substrates via DC magnetron sputtering by varying the vanadium target power from 20 W to 100 W. The influence of sputtering power on elemental composition, bonding states, and structural evolution was evaluated by x-ray photoelectron spectroscopy (XPS; survey and high-resolution C 1s/V 2p/O 1s), energy-dispersive x-ray spectroscopy (EDX), and x-ray diffraction (XRD). Elemental analysis revealed a non-linear increase in vanadium content with increasing target power. A significant discrepancy was observed between surface and bulk compositions: XPS indicated a maximum surface vanadium concentration of ∼7.8 at.% at 100 W, whereas EDX revealed a bulk concentration of up to 44.7 at.%. This divergence highlights pronounced surface oxidation. Deconvolution of high-resolution C 1s and V 2p XPS spectra confirmed a distinct structural transition. Films deposited at low powers (20–40 W) retained their amorphous carbon character with a relatively stable sp^2/sp^3 hybrid structure. In contrast, at high powers (70–100 W), the emergence of distinct spectral features at 282.5 eV (C 1s) and a low-binding-energy contribution near 513.5 eV (V 2p) is consistent with V–C bond formation at high target powers, supported by concurrent VC reflections in XRD. Overall, the data indicate a power-driven transition from an amorphous V-DLC network (20–40 W) to an nc-VC/a-C nanocomposite at 70–100 W.

1. Introduction

Diamond-like carbon (DLC) coatings are widely used in applications ranging from automotive components to biomedical implants because they combine high hardness, a low friction coefficient, chemical inertness, and biocompatibility [1–4]. The unique properties of DLC films stem from their amorphous structure, which consists of a mixture of sp^3-hybridized (diamond-like) and sp^2-hybridized (graphite-like) carbon bonds [2, 5]. The ratio of sp^3 to sp^2 bonds is the primary factor determining the mechanical and tribological performance of the coating [1, 5, 6].

Despite their superior properties, pure DLC films suffer from certain intrinsic limitations, particularly high compressive residual stress and poor adhesion to substrates, which restrict their widespread use in thick coating applications [1, 5, 7]. To mitigate these issues, the incorporation of various metallic dopants (e.g., Ti, Cr, W, V) into the carbon matrix has been extensively investigated [8–11]. Metal doping is known to reduce internal stress by relaxing the distorted bond angles and lengths in the atomic network, thereby enhancing adhesion and toughness, albeit often at the expense of hardness [8, 12–14].

Among various metal dopants, vanadium (V) is of particular interest due to its ability to form hard ceramic phases, such as vanadium carbide (VC), which can reinforce the coating structure [12, 15, 16]. Furthermore, vanadium-doped DLC (V-DLC) films have shown potential for improved tribological performance and oxidation resistance. However, the structural integration of vanadium into the amorphous carbon matrix is complex. Depending on the deposition conditions and dopant concentration, vanadium can either reside interstitially within the carbon network, form nanoclusters, or chemically react to form

© 2026 The Author(s). Published by IOP Publishing Ltd

carbide or oxide phases. Understanding the transition between these states is crucial for tailoring film properties [8, 12, 17, 18].

DC magnetron sputtering is a widely used technique for depositing metal-doped DLC films due to its scalability and good process controllability [10, 19]. In magnetron sputtering, target power was selected as the primary deposition variable because it directly controls both the flux and the kinetic energy of the sputtered metal species, thereby affecting not only the amount of vanadium incorporated into the film but also the energetic conditions at the growing surface [20]. Compared with other process variables such as working pressure or gas flow ratio, varying the target power provides a more direct route to probe changes in adatom mobility, bombardment intensity, and the likelihood of metal–carbon reaction during film growth. Since the present study specifically aims to track the transition from a dopant-modified amorphous network to a carbide-containing nanocomposite, target power was chosen as the main control parameter to isolate the energy-driven evolution of composition, bonding state, and phase formation [9, 13, 14, 21, 22].

In this study, V-DLC films were deposited by DC magnetron sputtering while systematically varying the vanadium target power from 20 W to 100 W. The primary objective is to establish a process–chemistry–structure map by correlating sputtering power with vanadium incorporation (surface versus bulk), the evolution of bonding states (V–C versus V–O), and the onset of crystalline VC precipitation and the accompanying morphology transition. XPS (survey and high-resolution C 1s, V 2p, and O 1s), EDX, and XRD were used to track composition, chemical state, and phase evolution. The present work is intentionally focused on chemical-state and structural evolution; quantitative mechanical or tribological testing is beyond the scope of this study.

Although Lai *et al* [22] reported the influence of sputtering conditions on pure DLC films, the present study addresses a fundamentally different case: a reactive V-doped carbon system in which target power governs not only structural rearrangement, but also vanadium incorporation, surface-to-bulk compositional divergence, chemical-state evolution, and the onset of crystalline VC precipitation. In this respect, the main contribution of the present work is to extend the sputtering-power discussion from undoped DLC to a dopant-reactive nanocomposite-forming system.

2. Materials and methods

2.1. Film deposition

V-DLC films were deposited on Si(100) substrates using a Nanovak NVTS-400 magnetron sputtering system via a co-deposition technique. Prior to deposition, the silicon substrates were ultrasonically cleaned in acetone and isopropyl alcohol sequentially, followed by rinsing with deionized (DI) water and drying with nitrogen gas. An indium-bonded pyrolytic graphite target ($\geqslant$99.999% purity, 2-inch diameter, 0.125-inch thickness) and a vanadium target (99.9% purity, 2-inch diameter, 0.125-inch thickness) were used as the carbon and metal sources, respectively. The vacuum chamber was evacuated to a base pressure better than 5.0×10^{-6} Torr prior to deposition to minimize background contamination. The high purity argon flow was controlled to maintain a working pressure of 3 mTorr.

The deposition conditions were controlled by varying the power applied to the vanadium target, while the carbon target was maintained at a constant DC condition (560 V/220 mA). The detailed deposition parameters and resulting film thicknesses for both series are summarized in table 1. In the first series, a pure DLC sample (0 W) was deposited for 10 h to achieve a sufficient thickness, while the V-doped samples (20, 30, and 40 W) were deposited for 4 h. The film thicknesses were measured using a KLA-Tencor P-17 stylus profilometer. In the second series, vanadium target powers of 40, 70, and 100 W were used, again with a constant deposition time of 4 h.

2.2. Characterization

The elemental composition and chemical bonding states of the films were analyzed by x-ray photoelectron spectroscopy (XPS) using a Thermo Scientific K-Alpha system equipped with a monochromatized Al Kα x-ray source (1486.6 eV). The analysis was performed with a spot size of 400 μm in standard lens mode. Survey spectra were acquired in constant analyzer energy mode with a pass energy of 150 eV and a step size of 1.0 eV, averaging 10 scans. High-resolution core-level spectra for C 1s, O 1s, and V 2p regions were recorded with a pass energy of 100 eV, a step size of 0.1 eV, and 20 scans. A pass energy of 100 eV was selected to optimize the signal-to-noise ratio without compromising chemical-state resolution. The binding energy scale was calibrated by referencing the sp^2 C 1s peak to 284.80 $\pm$ 0.05 eV. Spectral deconvolution was performed using a Shirley-type background and a Gaussian–Lorentzian mix (GL (30)) line shape, following the fitting principles described [17, 18].

Table 1. Deposition parameters and film thickness of pure and V-doped DLC samples.

Sample	V target power (W)	Thickness (μm) [a]	Deposition time (h)
Pure DLC	0	0.85	10
V-DLC 20 W	20	0.52	4
V-DLC 30 W	30	0.50	4
V-DLC 40 W (S1)	40	0.51	4
V-DLC 40 W (S2)	40	0.52	4
V-DLC 70 W	70	N.M.[b]	4
V-DLC 100 W	100	N.M.[b]	4

[a] SD $= \pm$ 0.01 μm.

[b] N.M., not measurable; film thickness could not be reliably determined by stylus profilometry for the samples exhibiting pronounced granular/cauliflower-like roughness (Series 2), due to the large height variations and ill-defined step edges.

Surface morphology and bulk elemental composition were investigated using a Thermo Scientific Quattro S scanning electron microscopy (SEM) equipped with an energy dispersive x-ray spectroscopy (EDX) module. SEM images were obtained at 100 k$\times$ magnification. EDX analyses were conducted at an accelerating voltage of 15 kV, a working distance of $\sim$10 mm, and spot size 4. Since XPS is surface-sensitive (probing the top few nanometers) while EDX is bulk-sensitive (probing micrometer depths), the comparative analysis of elemental composition was interpreted considering this surface-bulk depth difference.

Crystalline structure analysis was performed using x-ray diffraction (XRD) with a Cu Kα radiation source (λ = 1.5406 Å). The samples were scanned in Bragg–Brentano (θ–2θ) geometry within the 2θ range of 20°–80°, using a step size of 0.01° and a scan speed of 0.3 s/step. To enhance the visibility of minor peaks or shoulders characteristic of thin films, selected diffraction data were presented on a logarithmic y-axis scale.

Generative AI statement: AI tools (ChatGPT, OpenAI and Gemini, Google) were used to assist with language polishing (grammar and clarity) and the preparation of figure graphics based on author-provided experimental data. The AI tools were not used to generate or alter experimental data. All content was verified by the authors, who take full responsibility for the manuscript.

3. Results and discussion

3.1. Elemental composition and doping trends

The elemental composition of the pure and V-DLC films was investigated using XPS survey scans and EDX. Figure 1 illustrates the evolution of the XPS survey spectra as a function of the vanadium target power. All spectra exhibit a dominant C 1s peak at approximately 285 eV and an O 1s peak at $\sim$532 eV. The presence of oxygen is attributed to surface oxidation and adventitious contamination upon exposure to the atmosphere. As expected, the intensity of the V 2p peak (located in the 513–525 eV region) shows a strong correlation with the applied target power. While no vanadium signal is detected for the pure DLC sample, the V 2p peak becomes progressively more intense from 20 W to 100 W.

The atomic concentrations derived from the XPS survey spectra are summarized in table 2. The vanadium content increases non-linearly, from a trace level of 0.05 at.% at 20 W to 7.78 at.% at 100 W. This trend confirms that the co-deposition process effectively incorporates vanadium into the carbon matrix, with the doping level directly governed by the target power.

To gain a deeper insight into the elemental distribution throughout the film depth, the surface composition (obtained by XPS) was compared with the bulk composition (obtained by EDX) for all constituent elements, as presented in table 3. A notable discrepancy is observed between the two techniques, revealing distinct surface and bulk characteristics. For the highest doping level (100 W), XPS indicates a surface vanadium concentration of only $\sim$7.8 at.%, whereas EDX reveals a much higher bulk concentration of 44.7 at.%. Conversely, the carbon content exhibits an inverse trend. While the surface appears carbon-rich ($\sim$65.5 at.%) likely due to the adventitious carbon layer, the bulk analysis reveals a significant reduction in carbon content to $\sim$21.0 at.%. This stark contrast indicates that the high-power films develop a strongly depth-dependent composition, with a vanadium-rich bulk and a comparatively carbon/oxygen-enriched near-surface region within the XPS information depth. The high vanadium content measured by EDX represents the bulk micrometer-scale composition where carbide-rich

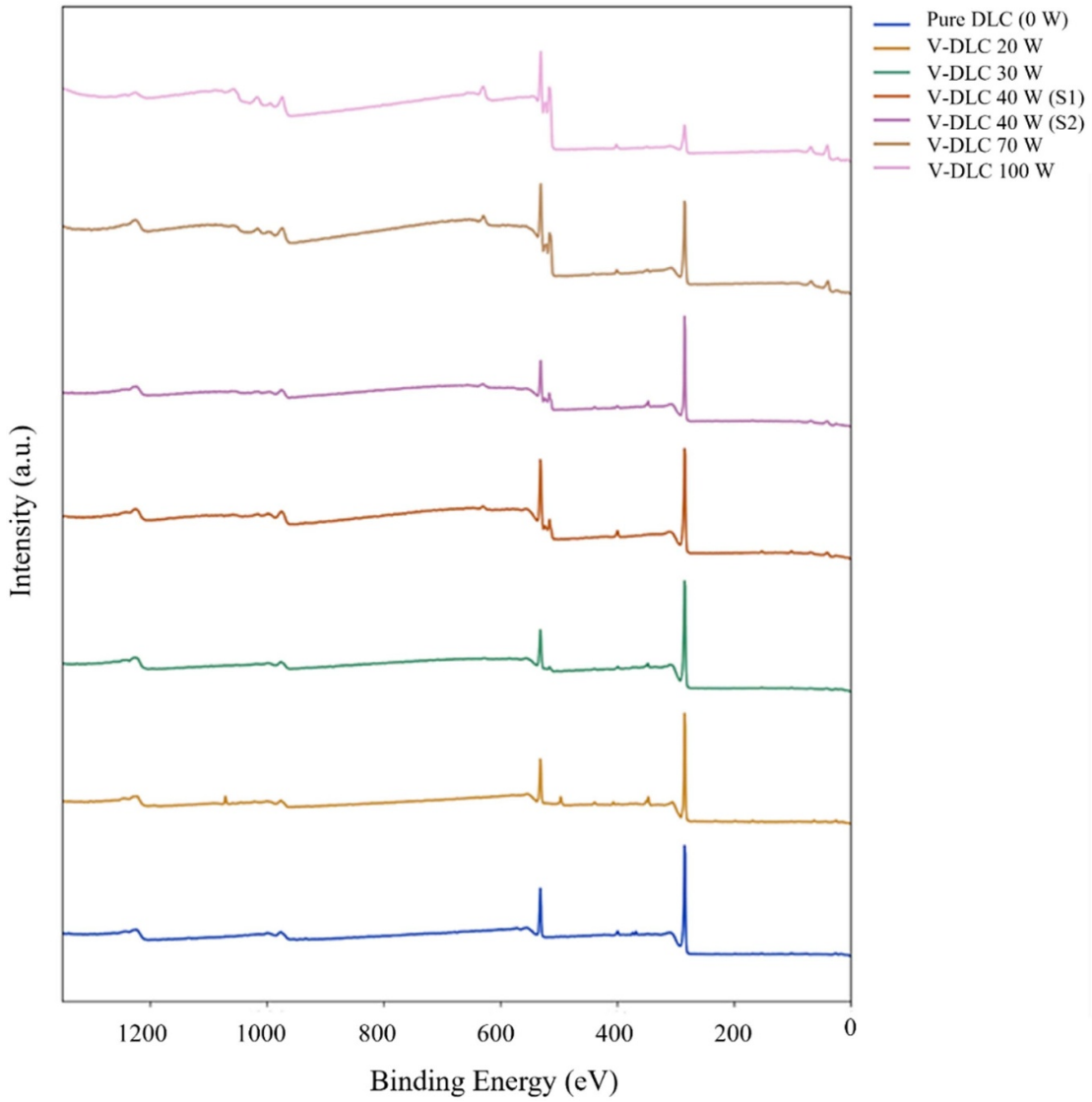

Figure 1. XPS survey spectra of pure and V-doped DLC films deposited at different target powers.

Table 2. Elemental composition of the films determined by XPS (at.%).

Sample	C (at.%)	O (at.%)	V (at.%)	Si (at.%)
Pure DLC	86.17	13.26	0.00	0.57
V-DLC 20 W	85.81	13.72	0.05	0.42
V-DLC 30 W	87.93	11.02	0.40	0.65
V-DLC 40 W (S1)	79.36	17.56	1.65	1.43
V-DLC 40 W (S2)	78.45	19.32	1.71	0.52
V-DLC 70 W	71.94	22.86	4.65	0.55
V-DLC 100 W	65.52	26.15	7.78	0.55

phases dominate, whereas XPS confirms that the near-surface region remains carbon-rich. Such disproportionately high bulk vanadium levels are typical for metal-rich nc-VC/a-C nanocomposites formed under high-power sputtering conditions and therefore do not contradict the DLC-like behavior observed at the surface [8, 10, 23–25].

The stark quantitative divergence between the surface (7.8 at.% V) and bulk (44.7 at.% V) concentrations at 100 W can be attributed to the strong attenuation of the V 2p photoelectron signal by the carbon- and oxygen-enriched near-surface region. Because XPS is limited to the outermost ∼5–10 nm, the high surface carbon (65.5 at.%) and oxygen (26.2 at.%) contents dominate the measured signal. Based on the O 1s and V 2p deconvolution results, this near-surface region is more reasonably interpreted as a mixed surface layer containing adventitious carbon together with vanadium oxide species,

Table 3. Comparison of elemental composition (at.%) obtained from surface-sensitive XPS and bulk-sensitive EDX analyses.

Sample	C (XPS)	C (EDX)	O (XPS)	O (EDX)	V (XPS)	V (EDX)
Pure DLC	86.2	71.4	13.3	28.6	0.0	0.0
V-DLC 20 W	85.8	65.9	13.7	33.5	0.1	0.6
V-DLC 30 W	87.9	61.3	11.0	34.8	0.4	3.9
V-DLC 40 W (S1)	79.4	54.6	17.6	38.2	1.7	7.2
V-DLC 40 W (S2)	78.5	61.0	19.3	28.4	1.7	10.6
V-DLC 70 W	71.9	27.6	22.9	39.0	4.7	33.4
V-DLC 100 W	65.5	21.0	26.2	34.3	7.8	44.7

rather than as a single, fully continuous oxide layer of defined thickness. Although the exact physical thickness of this mixed near-surface region cannot be determined from the present data, its influence clearly falls within the XPS information depth and substantially suppresses the apparent contribution of the underlying vanadium-rich bulk nanocomposite to the measured surface composition. Thus, the XPS–EDX discrepancy is not contradictory; rather, it indicates a pronounced depth-dependent compositional gradient, consisting of a carbon/oxygen-enriched near-surface region above a vanadium-rich bulk. For the 100 W film, the V(EDX)/V(XPS) ratio is approximately 5.7, quantitatively underscoring the pronounced surface-to-bulk compositional mismatch associated with near-surface oxidation and bulk vanadium enrichment. The carbide-related XPS features increase systematically with sputtering power, demonstrating that they are intrinsic to the film rather than arising from random surface contamination. The high oxygen content observed in both XPS and EDX for high-power samples suggests that vanadium acts as a strong oxygen getter during the deposition process or post-deposition air exposure, leading to the formation of vanadium oxides within the film structure [17, 18]. Furthermore, such a depth-dependent composition may influence the functional response of the coatings. The carbon/oxygen-enriched near-surface region is expected to govern the initial contact chemistry and may help reduce interfacial shear relative to a fully metal-rich surface, whereas the vanadium-rich, carbide-containing subsurface can provide greater load-bearing support and resistance to subsurface deformation. In this sense, the coexistence of a comparatively carbon-rich surface and a carbide-rich bulk may be beneficial for combining low-friction surface behavior with improved mechanical robustness, as often discussed for metal-doped DLC and carbide/a-C nanocomposite coatings [1, 8, 15, 24]. However, because no direct tribological or nanoindentation measurements were performed in the present study, these implications should be regarded as plausible structure–property consequences rather than experimentally verified performance gains.

3.2. Chemical bonding and structural evolution

The bonding configuration of DLC films, particularly the sp^3/sp^2 hybridization, is a key descriptor of their structure. Introducing a reactive metal such as vanadium can further induce competing carbide and oxide chemistries within the carbon matrix. To elucidate the structural evolution and identify the chemical states of the constituent elements, the high-resolution XPS spectra of C 1s, V 2p, and O 1s were analyzed in detail.

3.2.1. Carbon hybridization and carbide formation (C 1s analysis)

The structural evolution of the carbon matrix as a function of target power was first investigated by examining the qualitative trends in the C 1s core-level spectra. Figure 2 displays the stacked (waterfall) C 1s spectra for the pure and V-doped DLC films.

As evident in figure 2, the spectral profiles exhibit a clear dependence on the sputtering power. The spectrum of the pure DLC sample is symmetric and centered at approximately 284.4 eV, which is typical for amorphous carbon films [5, 26]. For the low-power doped samples (20–40 W), the peak shape remains largely preserved, suggesting that the incorporation of small amounts of vanadium does not drastically disrupt the carbon network. However, a significant spectral transformation occurs at 70 W and 100 W. A distinct broadening towards the lower binding energy side is observed, leading to the emergence of a well-defined 'shoulder' at ∼282.5 eV. This low-energy feature is a spectroscopic fingerprint of vanadium–carbon (V–C) bonds, indicating the nucleation of a carbide phase [12, 23, 27]. Additionally, the progressive sharpening and intensity increase of this feature with higher sputtering power further supports its intrinsic carbide origin. While the 282.5 eV shoulder is consistent with V–C bonding reported in the literature, it can also overlap with subcarbide or interfacial V–C states.

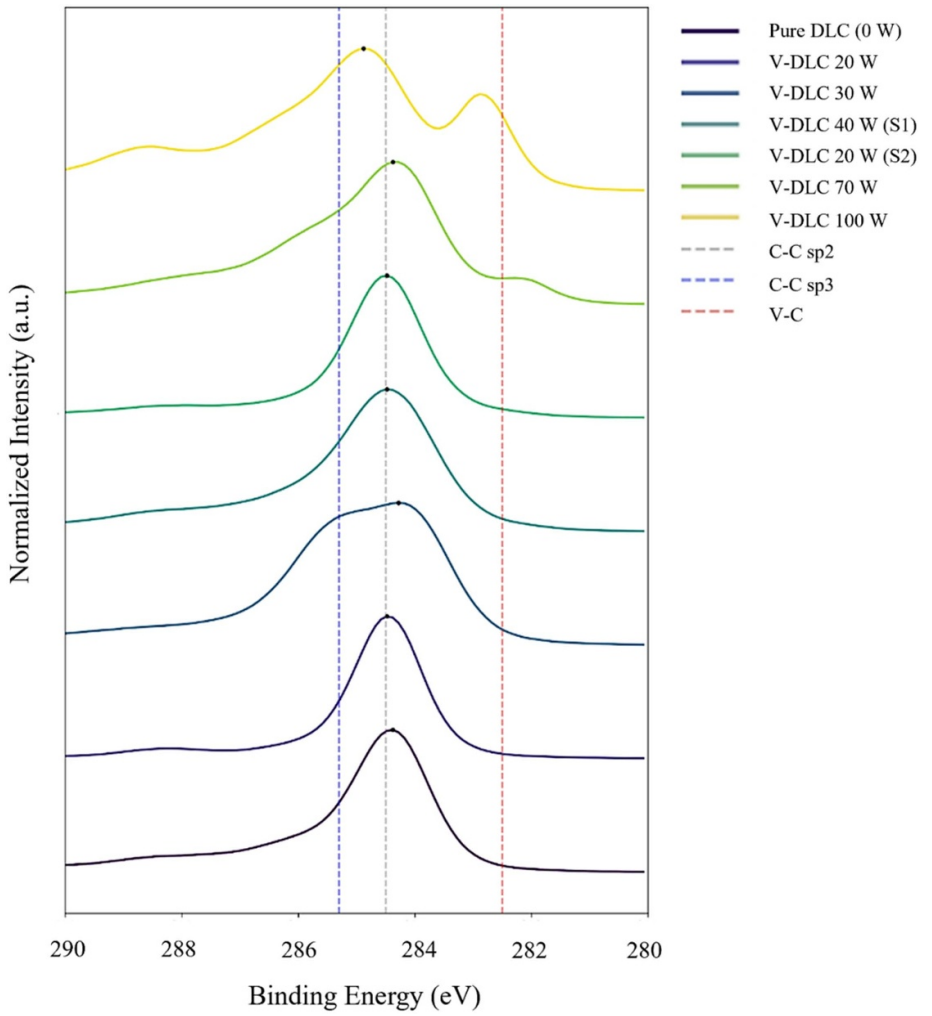

Figure 2. Stacked high-resolution C 1s XPS spectra of pure and V-doped DLC films. The vertical dashed lines indicate the binding energy positions for vanadium carbide (V–C, ∼282.5 eV) and the main C–C/C=C band (∼284.5 eV).

Therefore, the carbide assignment is based on the combined evidence of C 1s, V 2p, and XRD. To quantify these structural changes, the C 1s spectra were mathematically deconvoluted using mixed Gaussian–Lorentzian functions. The fitted spectra for all samples are presented in figure 3.

The quantitative results derived from these fits, including the relative area percentages of each component, are summarized in table 4.

The deconvolution analysis reveals two distinct regimes of structural evolution. In the low-power regime (20–40 W), the films retain their DLC character. The sp^3 content fluctuates in the range of 20–36%, indicating that vanadium atoms are primarily dispersed within the amorphous matrix or occupy interstitial sites without forming a continuous carbide network. The fluctuation in apparent sp^3 content can be understood in terms of the changing growth energetics as the vanadium target power increases. Higher sputtering powers increase both the flux and the kinetic energy of the arriving species, which can enhance subplantation, local compressive stress, and short-range bonding rearrangements within the amorphous carbon matrix. A similar power-driven sensitivity of DLC structure and morphology has been reported for sputtered DLC films, where increasing target power altered the sp^3/sp^2 balance and promoted structural rearrangement under more energetic bombardment. In the present V-DLC system, these effects likely contribute to the low-power variations in the apparent sp^3 fraction, whereas in the high-power regime (70–100 W) the dominant process shifts toward vanadium–carbon reaction and carbide precipitation. Therefore, the C 1s-derived sp^3/sp^2 values should be interpreted as qualitative indicators of relative bonding rearrangement rather than as absolute measures of diamond-like character [6, 22, 26, 28]. Unlike the pure-DLC behavior discussed by Lai *et al* [22], the high -power response in the present V-DLC system is coupled to vanadium-mediated carbide formation, as evidenced by the concurrent emergence of the carbide-related C 1s shoulder, the low-binding-energy (low-BE) V 2p contribution, and the VC reflections in XRD.

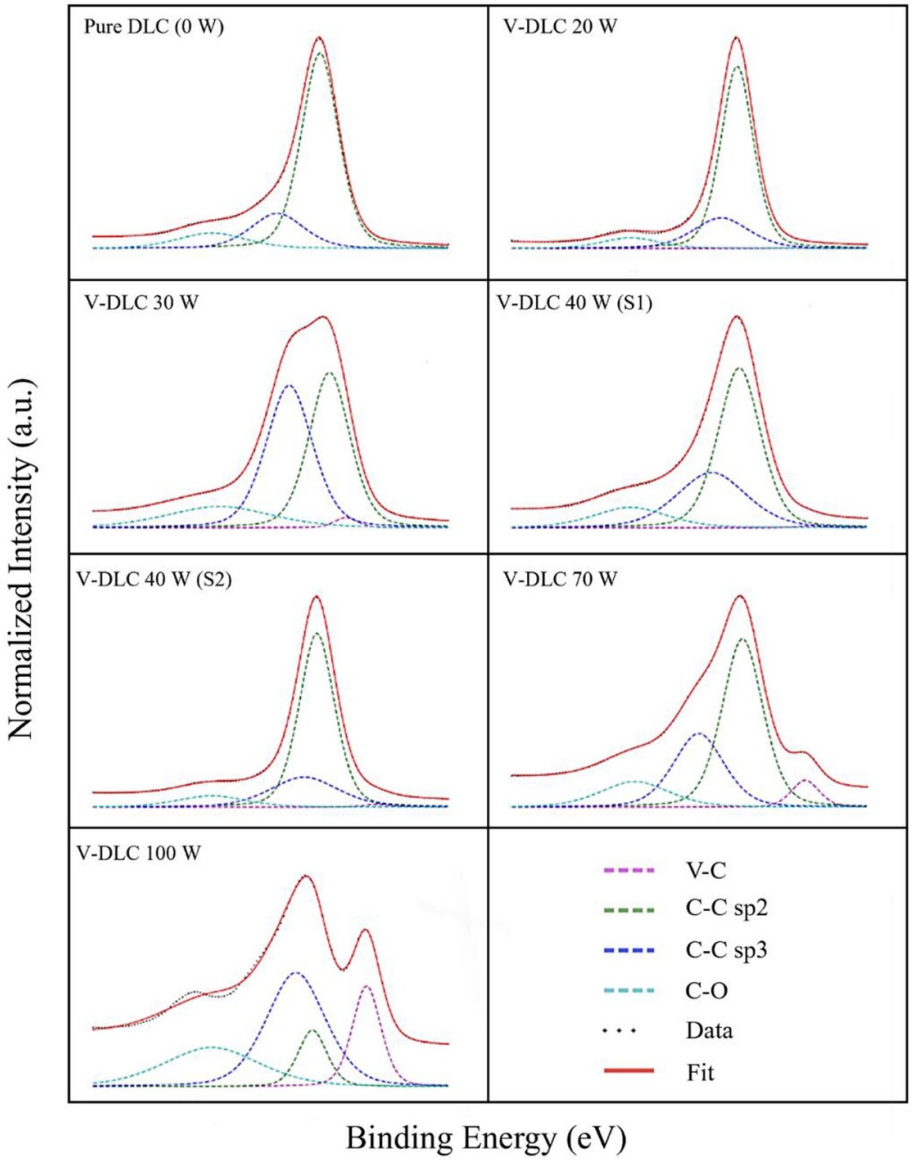

Figure 3. Deconvoluted C 1s spectra of the films showing the sub-components: sp^2 (C=C), sp^3 (C–C), C–O contaminants, and the V–C carbide phase. All spectra are presented within the binding energy window of 292–280 eV.

Table 4. Deconvolution results of C 1s spectra (Area %).

Sample	V–C %	sp2 (C=C) %	sp3 (C–C) %	C–O/C=O %	sp3 Ratio (%)
Pure DLC	0.0	71.5	18.2	10.3	20.3
V-DLC 20 W	0.1	72.2	20.5	7.1	22.1
V-DLC 30 W	1.5	41.1	43.0	14.4	51.1
V-DLC 40 W (S1)	0.3	55.9	31.5	12.3	36.0
V-DLC 40 W (S2)	0.8	68.1	22.5	8.6	24.8
V-DLC 70 W	5.7	52.4	28.4	13.5	35.2
V-DLC 100 W	19.2	10.9	45.0	24.9	80.5

In the high-power regime (70–100 W), the V-C component increases dramatically, reaching ∼19.2% for the 100 W sample. This confirms that the high kinetic energy of the sputtered atoms at 100 W overcomes the activation barrier for the chemical reaction between V and C, leading to the formation of a stable VC phase. Consequently, the material transforms from a metal-doped DLC film into a metal-carbide-reinforced nanocomposite [8, 20, 24, 29, 30]. It should be emphasized that the high apparent sp^3 ratio for the 100 W sample should not be interpreted as a genuine enhancement of diamond-like character. Rather, it is most likely influenced by spectral overlap among carbide-, oxide-, and sp^3-related contributions, while the dominant structural change in this regime is the precipitation of the carbide phase.

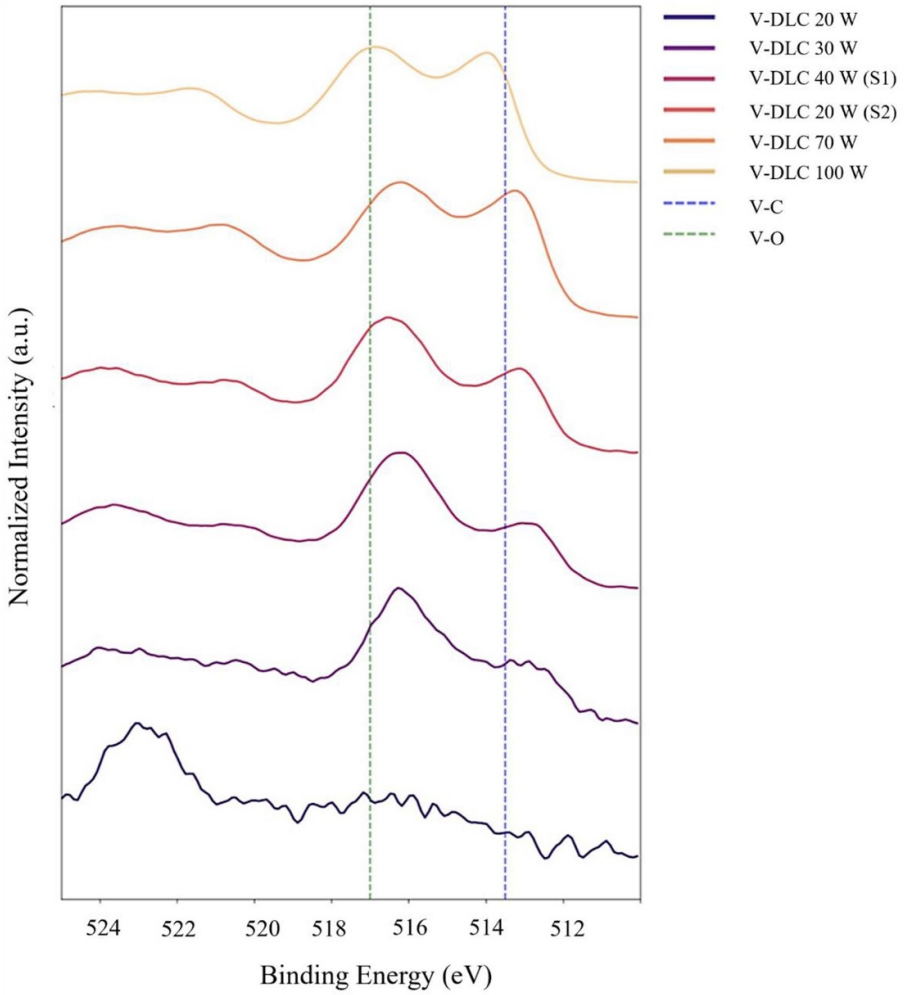

Figure 4. Stacked high-resolution V 2p XPS spectra showing the emergence of a low-binding-energy feature (∼513.5 eV) at high target powers.

While Raman spectroscopy is often employed to analyze the bulk disorder and I_D/I_G ratio in DLC films, XPS offers the distinct advantage of directly probing the chemical bonding environment of the dopant species. Since the primary focus of this study is the chemical interaction between Vanadium and Carbon (specifically the V-C bond formation) rather than the bulk sp^3 fraction, the C 1s core-level analysis provides the necessary chemical state resolution to confirm the carbide phase precipitation.

3.2.2. Vanadium chemical state (V 2p analysis)

To corroborate the carbide formation observed in the C 1s spectra, the chemical state of vanadium was analyzed using the V 2p core-level spectra. Figure 4 illustrates the evolution of the stacked V 2p spectra.

The V 2p spectra exhibit a clear shift in the dominant chemical state. For the low-power samples (20–30 W), the signal is dominated by a peak centered at ∼517.0 eV. This binding energy corresponds to vanadium oxide (V–O) species (such as V_2O_5 or VO_2), indicating that the surface vanadium atoms are heavily oxidized upon exposure to the atmosphere. However, as the target power increases to 70 W and 100 W, a new spectral feature becomes prominent at a lower binding energy of ∼513.5 eV (indicated in figure 4). Although the 513.5 eV feature can overlap with lower-valence vanadium oxides (e.g., VO), its concurrent appearance with the 282.5 eV C 1s shoulder and the VC diffraction peaks suggests that it is primarily associated with V–C bonding in the high-power regime.

The detailed deconvolution of these spectra is presented in figure 5, and the calculated phase fractions are listed in table 5.

The fitting results confirm a dominant oxidized vanadium component and a low-BE contribution near ∼513.5 eV. Because this region can overlap with low-valence vanadium oxides (e.g., VO), the low-BE component is interpreted cautiously for the low-power films (20–40 W). For the high-power films (70–100 W), the low-BE component was interpreted by considering the combined evidence rather than

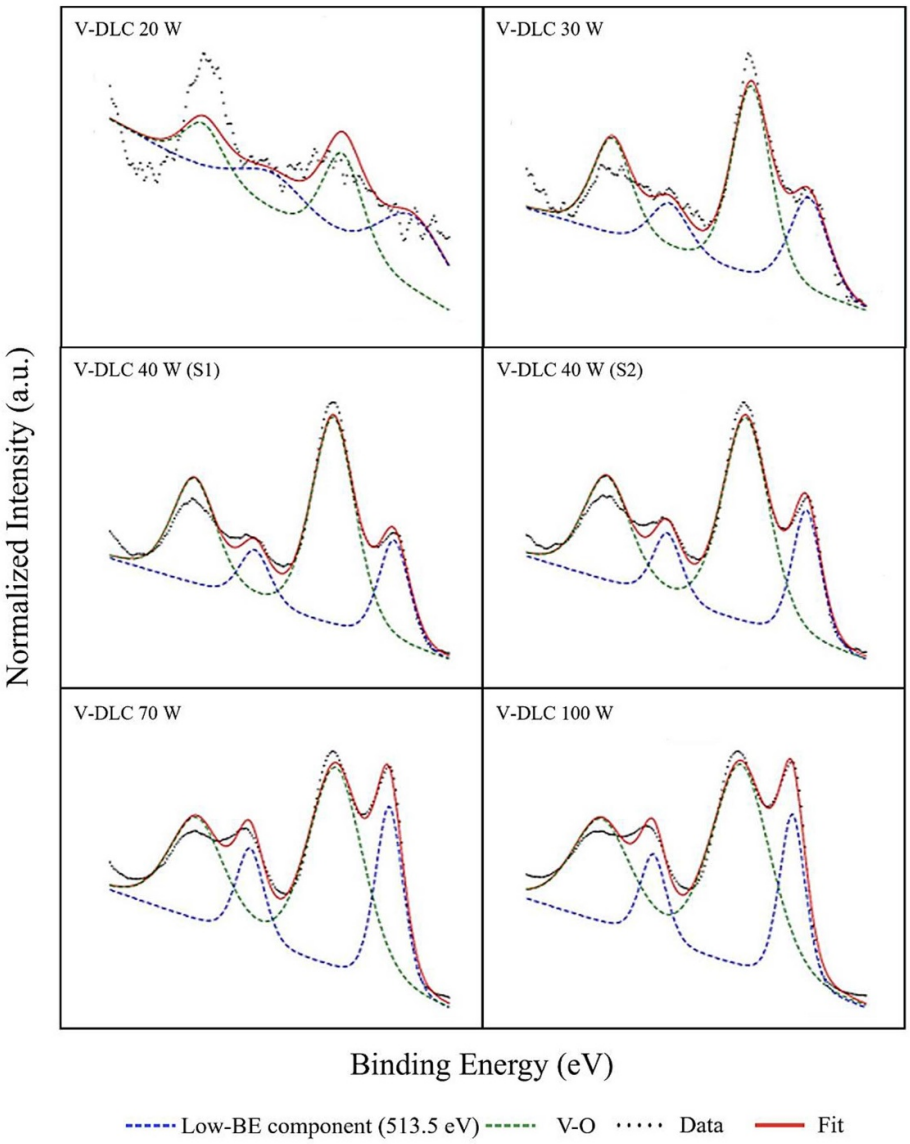

Figure 5. Deconvoluted V 2p XPS spectra showing the relative contributions of the low-binding-energy component (∼513.5 eV; V–C/VO overlap) and vanadium oxide (V–O) components. All spectra are presented within the binding energy window of 527.5–510 eV.

Table 5. Deconvolution results of V 2p spectra (Area %).

Samples	Low-BE component (∼513.5 eV) [a]	V-O (Oxide)
V-DLC 20 W	N.D.[b]	100
V-DLC 30 W	33.5	66.5
V-DLC 40 W (S1)	26.1	73.9
V-DLC 40 W (S2)	28.4	71.6
V-DLC 70 W	31.5	68.5
V-DLC 100 W	27.3	72.7

[a] N.D. (not detected): low-BE component was not detected within the fitting limits/noise level.

[b] Low-BE component (∼513.5 eV): may include contributions from V–C and/or low-valence VO; for 70–100 W films it is assigned primarily to V–C based on the concurrent C 1s carbide feature and VC reflections in XRD.

the V 2p binding energy alone. In these samples, the distinct C 1s shoulder at ∼282.5 eV, which is associated with carbide-related bonding, appears together with the VC reflections in the XRD patterns, whereas both features are absent in the pure DLC and low-power films. The simultaneous emergence of

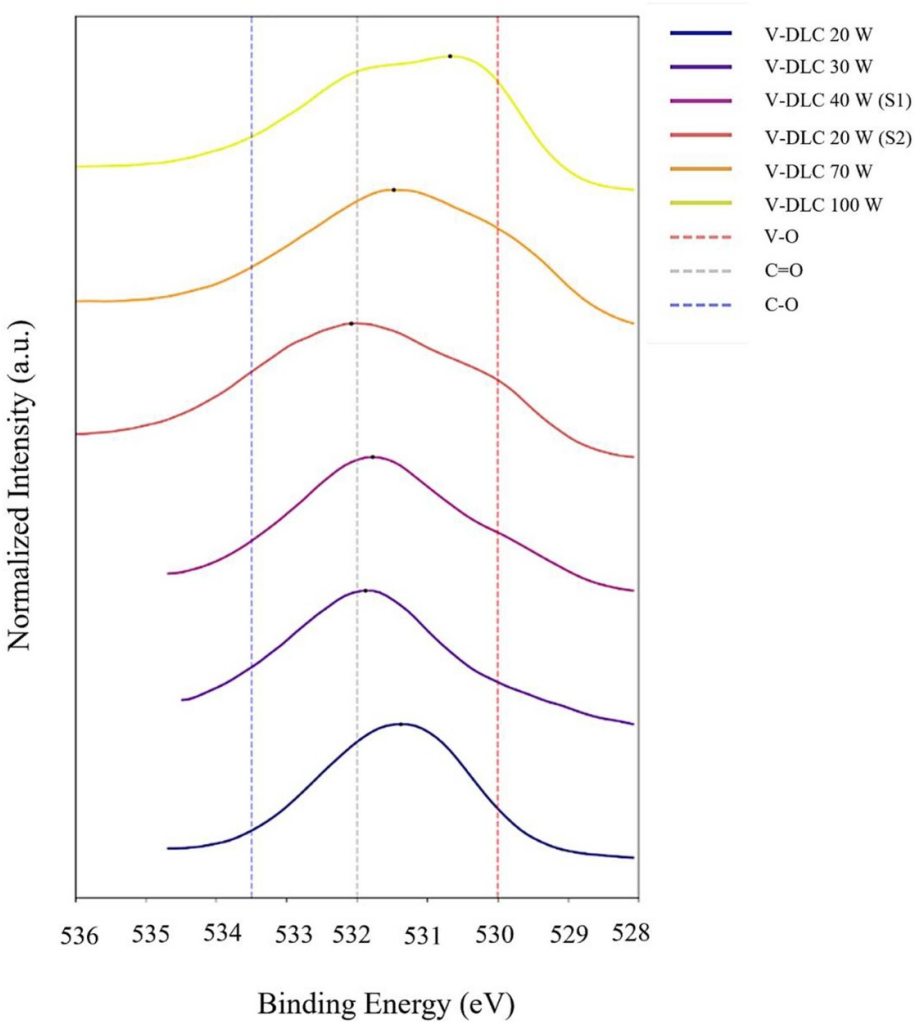

Figure 6. Stacked high-resolution O 1s XPS spectra showing a significant negative binding energy shift at 100 W.

these independent signatures only in the high-power regime supports assigning the ∼513.5 eV component primarily to V–C bonding within the XPS information depth. However, since partial overlap with low-valence vanadium oxides cannot be completely ruled out, this assignment is presented as the dominant interpretation rather than the only possible one [13, 27].

3.2.3. Oxygen bonding nature (O 1s analysis)

Finally, the O 1s spectra were analyzed to identify the source of oxygen within the films. Figure 6 shows the stacked O 1s spectra, and figure 7 presents the deconvoluted components.

For the low-power samples (20–40 W), the O 1s peak is located at ∼532.0 eV, which is characteristic of organic C–O or C=O bonds [17, 18]. This suggests that for low doping levels, oxygen is primarily present as surface contamination or is adsorbed on the carbon network. No significant O–C=O component was detected in the 533–534 eV region, confirming that oxygen mainly exists as C–O/C=O species and V–O oxides [17, 18].

Notably, for the 100 W sample, the O 1s peak shifts to a lower binding energy of 530.68 eV. As detailed in table 6, the deconvolution reveals a sharp increase in the metal-oxide (V–O) component (∼26%).

This result indicates a clear change in the near-surface chemistry at high target powers. The observed gettering behavior likely involves contributions from both deposition-stage oxygen uptake and post-deposition atmospheric oxidation. During sputtering, highly reactive vanadium species may interact with residual oxygen-containing species present in the chamber at the base pressure used in this study (∼5.0×10^{-6} Torr), leading to oxygen incorporation into the film and contributing to the elevated oxygen content detected by EDX. After deposition, subsequent exposure of the vanadium-rich near-surface region to air likely promotes additional oxidation, which contributes strongly to the V–O

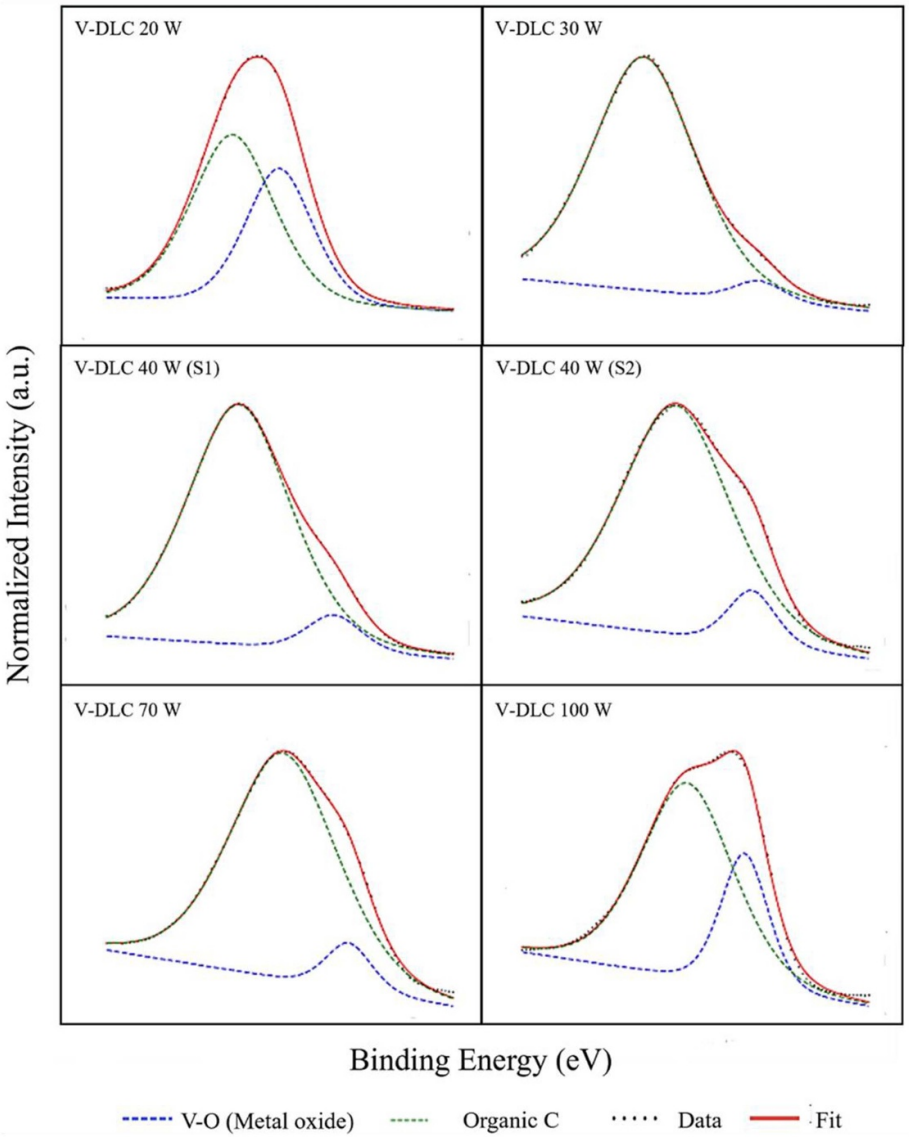

Figure 7. Deconvoluted O 1s spectra showing the transition from organic oxygen (C–O) to metal oxide (V–O). All spectra are presented within the binding energy window of 536–527 eV.

Table 6. Deconvolution results of O 1s spectra (Area %).

Sample	V–O (Metal oxide)	Organic O (C–O/C=O)
V-DLC 20 W	—	∼100.0
V-DLC 30 W	4.1	95.9
V-DLC 40 W (S1)	7.4	92.6
V-DLC 40 W (S2)	9.4	90.6
V-DLC 70 W	8.2	91.8
V-DLC 100 W	26.1	73.9

component observed by XPS. Therefore, the oxygen signal in the high-power films is more reasonably interpreted as the combined result of bulk-related oxygen incorporation during deposition and further near-surface oxidation after atmospheric exposure, rather than as arising from only one of these two processes [17, 18].

3.3. Crystalline structure (XRD analysis)

The crystalline structure of the films was investigated by XRD to confirm the presence of the carbide phase suggested by XPS. Figure 8 shows the XRD patterns of the pure and V-doped DLC films.

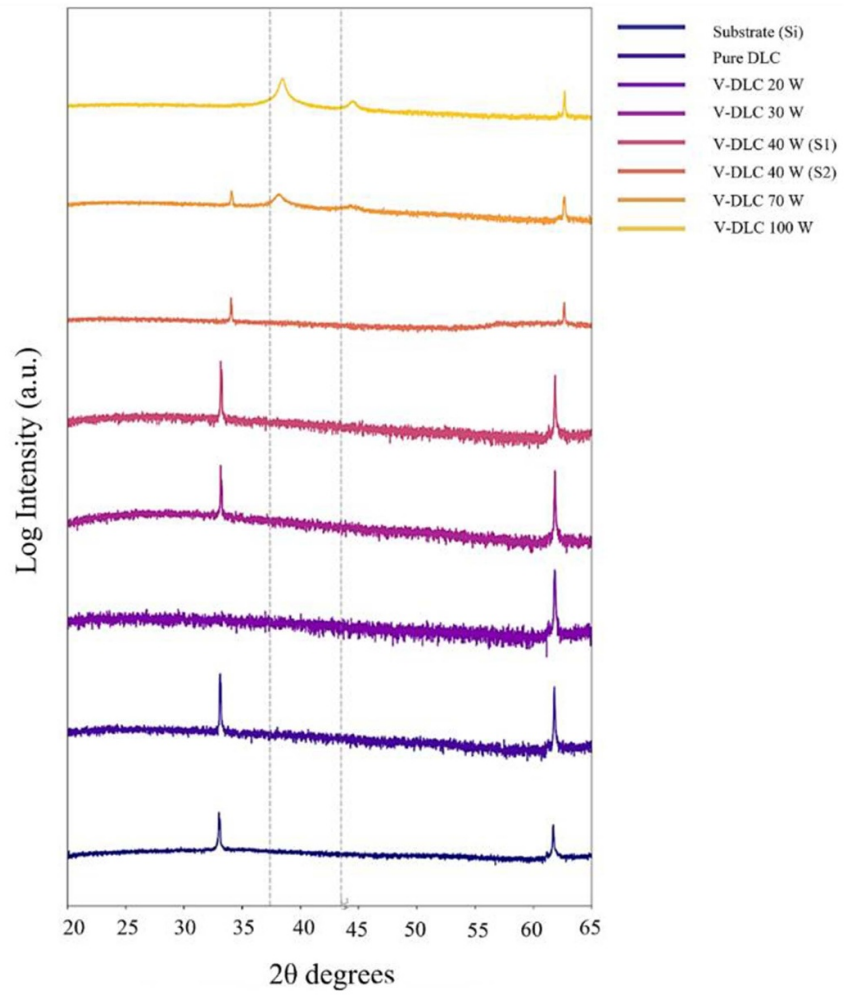

Figure 8. XRD patterns of V-DLC films deposited at different target powers. The vertical dashed lines indicate the standard positions for cubic vanadium carbide (VC).

The pure DLC and low-power doped samples (20–40 W) exhibit no distinct diffraction peaks, showing only a broad hump characteristic of an amorphous carbon structure [1, 5]. Two substrate-related peaks are consistently observed at ∼33.0° and ∼61.7° in all samples, originating from the Si wafer.

In contrast, for the 70 W and 100 W samples, new diffraction features emerge. A distinct peak is observed near ∼43.8°, which corresponds to the (200) plane of the face-centered cubic VC phase. A weaker feature is also discernible near ∼37.8 °, corresponding to the (111) plane. Although the VC reflections exhibit low intensity due to the nanocrystalline and low-volume-fraction nature of the carbide phase, their reproducibility across repeated scans and alignment with standard VC positions confirm their validity. It is notable that these experimental peaks are shifted slightly to higher angles (right shift) compared to the standard bulk VC values (43.5° and 37.4°, JCPDS 00–035–0786). This shift may be related to compressive residual stress in the film and/or a non-stoichiometric carbide composition (VCx), as commonly discussed for sputtered nanocomposite films. Such right-shifted VC peaks have been widely reported in sputtered carbide films and are often associated with lattice contraction caused by compressive residual stress and/or carbon-rich VC_x stoichiometry [25, 29, 31]. However, no independent verification of residual stress or exact nanocluster stoichiometry was performed in the present study. Therefore, these explanations should be regarded as plausible literature-supported interpretations rather than direct proof. Nevertheless, the reproducible emergence of the VC reflections still confirms the precipitation of crystalline VC nanoclusters within the amorphous matrix at high sputtering powers [30, 32, 33].

The average crystallite size of the VC phase in the 100 W sample was estimated using the Scherrer equation based on the (200) peak broadening. The calculated crystallite size is approximately 6.4 nm.

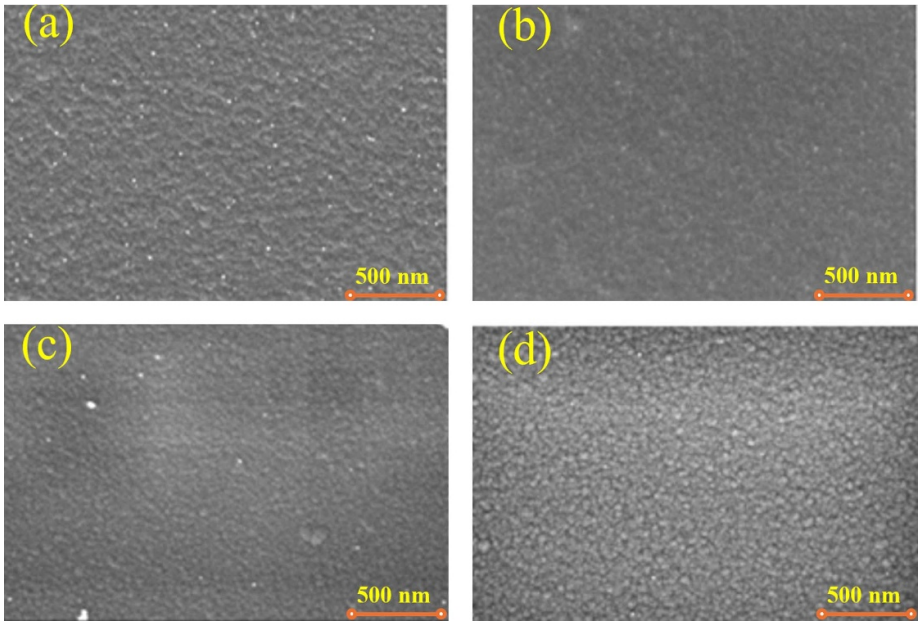

Figure 9. SEM surface micrographs (100 k×) of the Series 1 samples: (a) Pure DLC, (b) V-DLC 20 W, (c) V-DLC 30 W, and (d) V-DLC 40 W (S1).

This nanocrystalline nature supports the formation of a nc-VC/a-C nanocomposite structure, consistent with the granular morphology observed in SEM images [23, 25].

3.4. Surface morphology analysis

The evolution of the surface morphology as a function of vanadium target power was investigated using SEM. To clearly visualize the effect of doping regimes, the micrographs are presented in two sets: figure 9 illustrates the low-power doping series (series 1), while figure 10 displays the high-power doping series (series 2).

The pure DLC film (figure 9(a)) exhibits a smooth, dense, and featureless surface morphology, which is characteristic of amorphous carbon films. This 'glassy' appearance indicates a lack of long-range crystalline order and grain boundaries, consistent with the XRD results showing only a broad amorphous hump.

As shown in figures 9(b)–(d), the films deposited at low vanadium powers (20–40 W) largely retain this smooth and homogeneous morphology. Although a very subtle textural change can be observed at 40 W, the surface remains free of distinct grains or clusters. This suggests that in the low-power regime, the doped vanadium atoms are effectively dissolved within the amorphous carbon matrix or occupy interstitial sites without inducing significant segregation or crystallization. The preservation of the smooth morphology confirms that doping at these levels does not significantly disrupt the continuous amorphous carbon network.

In stark contrast, a drastic morphological transformation is observed in the second series as the target power increases (figure 10). While the 40 W sample (figure 10(b)) still exhibits a smooth surface similar to Series 1, the films deposited at 70 W (figure 10(c)) and 100 W (figure 10(d)) lose their featureless character completely. The surface develops a pronounced granular structure with a 'cauliflower-like' morphology, characterized by distinct agglomerates and increased roughness [25, 31].

This microstructural coarsening observed at high target powers can be attributed to two synergistic factors. First, the precipitation and growth of crystalline VC—supported by the sharp VC reflections in XRD and the concurrent emergence of V–C-related features in XPS—progressively disrupt the amorphous continuity of the DLC matrix, resulting in a more textured and granular surface. Second, increasing the target power (up to 100 W) enhances both the flux and the kinetic energy of sputtered vanadium species, which increases adatom mobility during deposition and promotes the coalescence of nucleated clusters into larger grains [20, 22].

These SEM observations provide strong visual confirmation of the structural transition from a dopant-modified amorphous coating to a nanocrystalline-carbide/amorphous-carbon nanocomposite structure [23, 24, 27, 33]. A similar transition from an amorphous to a nanocrystalline nanocomposite structure has also been reported for Ti- and W-doped diamond-like nanocomposite films [34, 35].

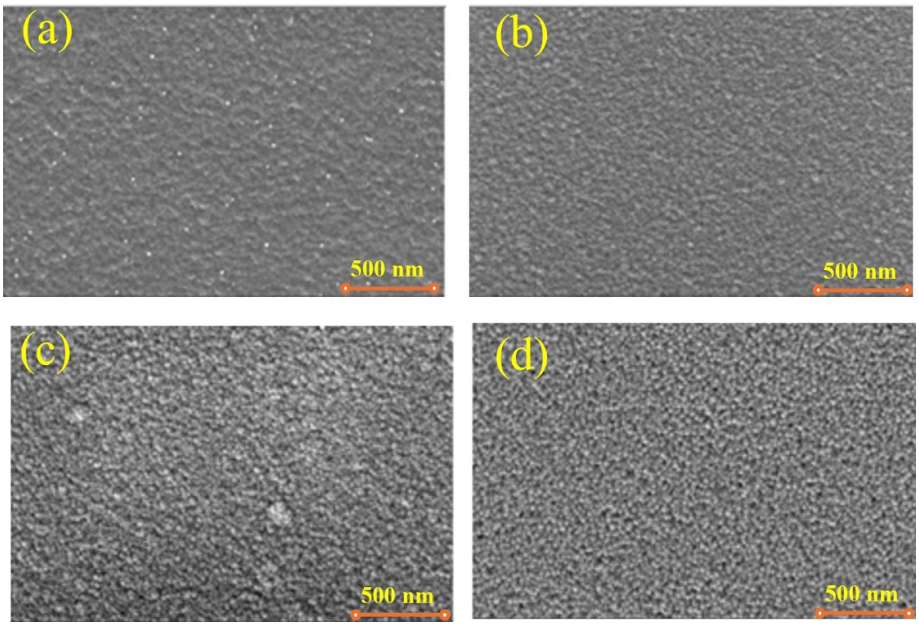

Figure 10. SEM surface micrographs (100 k×) of the Series 2 samples: (a) Pure DLC, (b) V-DLC 40 W (S2), (c) V-DLC 70 W, and (d) V-DLC 100 W.

Although quantitative roughness or grain-size analysis was not performed, the consistent emergence of granular/cauliflower-like features at 70–100 W across multiple micrographs supports a coarsening process associated with carbide nucleation and growth.

4. Conclusions

In summary, this study establishes a process–chemistry–structure framework for V-doped DLC films by showing how vanadium target power governs vanadium incorporation, chemical-state evolution, phase formation, and morphology. The results reveal a clear transition from a dopant-modified amorphous carbon network in the low-power regime (20–40 W) to an nc-VC/a-C nanocomposite in the high-power regime (70–100 W), as evidenced by the concurrent emergence of carbide-related C 1s and V 2p features, crystalline VC reflections in XRD, and granular/cauliflower-like surface morphology.

A key contribution of this work is the combined identification of two simultaneous but distinct phenomena occurring at high target powers: bulk carbide formation and pronounced surface-to-bulk compositional divergence caused by vanadium's oxygen affinity. In this respect, the study shows that sputtering power acts not only as a compositional parameter, but also as a decisive control variable for the chemical state and structural architecture of V-DLC coatings.

These findings provide a useful basis for the design of multifunctional coatings in which a carbon/oxygen-enriched near-surface region coexists with a vanadium-rich, carbide-containing bulk. Although direct tribological and mechanical testing was beyond the scope of the present study, the identified structural evolution offers a rational guide for future optimization of hardness, wear resistance, and other functional properties.

Acknowledgments

This work was supported by the Scientific Research Projects Unit of Marmara University under the ADEP project (Project No. ADF-2023-10860).

Data availability statement

The data that support the findings of this study are available upon reasonable request from the authors. The datasets were generated specifically for this study and are currently retained by the authors and the

relevant laboratory. They have not been deposited in a public repository because the data consist mainly of instrument-generated characterization files and processed analysis files, and no dedicated public repository was used during the submission process. However, the data supporting the findings and conclusions of the manuscript are available from the corresponding author upon reasonable request.

ORCID iDs

Görkem Yumuşak 0000-0002-5047-4357
Bahadır Tunaboylu 0000-0001-9928-8689

References

[1] Erdemir A and Donnet C 2006 Tribology of diamond-like carbon films: recent progress and future prospects *J. Phys. D: Appl. Phys.* **39** R311
[2] Lifshitz Y 1999 Diamond-like carbon—present status *Diam. Relat. Mater.* **8** 1659–76
[3] Hauert R, Thorwarth K and Thorwarth G 2013 An overview on diamond-like carbon coatings in medical applications *Surf. Coat. Technol.* **233** 119–30
[4] Malisz K, Świeczko-żurek B and Sionkowska A 2023 Preparation and characterization of diamond-like carbon coatings for biomedical applications—a review *Materials* **16** 3420
[5] Robertson J 2002 Diamond-like amorphous carbon *Mater. Sci. Eng. R* **37** 129–281
[6] Ferrari A C and Robertson J 2000 Interpretation of Raman spectra of disordered and amorphous carbon *Phys. Rev. B* **61** 14095
[7] Bewilogua K and Hofmann D 2014 History of diamond-like carbon films—From first experiments to worldwide applications *Surf. Coat. Technol.* **242** 214–25
[8] Yetim A F, Kovacı H, Kasapoğlu A E, Bozkurt Y B and Çelik A 2021 Influences of Ti, Al and V metal doping on the structural, mechanical and tribological properties of DLC films *Diam. Relat. Mater.* **120** 108639
[9] Gayathri S, Kumar N, Krishnan R, Ravindran T R, Amirthapandian S, Dash S, Tyagi A K and Sridharan M 2015 Influence of transition metal doping on the tribological properties of pulsed laser deposited DLC films *Ceram. Int.* **41** 1797–805
[10] Flege S, Hatada R, Hanauer A, Ensinger W, Morimura T and Baba K 2017 Preparation of metal-containing diamond-like carbon films by magnetron sputtering and plasma source ion implantation and their properties *Adv. Mater. Sci. Eng.* **2017** 9082164
[11] Kalin M, Vižintin J, Barriga J, Vercammen K, van Acker K and Arnšek A 2004 The effect of doping elements and oil additives on the tribological performance of boundary-lubricated DLC/DLC contacts *Tribol. Lett.* **17** 679–88
[12] Li H, Hu J, Lin G and Dong C 2010 V and N co-doped diamond-like carbon films deposited by pulsed bias arc ion plating *Int. J. Refract. Met. Hard Mater.* **28** 544–9
[13] Zhou Y, Li L, Shao W, Chen Z, Wang S, Xing X and Yang Q 2020 Mechanical and tribological behaviors of Ti-DLC films deposited on 304 stainless steel: exploration with Ti doping from micro to macro *Diam. Relat. Mater.* **107** 107870
[14] Jing P P, Ma D L, Gong Y L, Luo X Y, Zhang Y, Weng Y J and Leng Y X 2021 Influence of Ag doping on the microstructure, mechanical properties, and adhesion stability of diamond-like carbon films *Surf. Coat. Technol.* **405** 126542
[15] Tekdir H and Yetim A F 2025 Multi-pass scratch properties of titanium and vanadium-doped diamond-like carbon coatings applied on commercially pure titanium under different tribological environments: dry, bio-aqueous, and lubricated conditions *Mater. Lett.* **398** 138913
[16] Shigemoto A, Amano T and Yamamoto R 2014 Work function measurements of vanadium doped diamond-like carbon films by ultraviolet photoelectron spectroscopy (arXiv: 1402.1911)
[17] Biesinger M C, Lau L W M, Gerson A R and Smart R S C 2010 Resolving surface chemical states in XPS analysis of first row transition metals, oxides and hydroxides: sc, Ti, V, Cu and Zn *Appl. Surf. Sci.* **257** 887–98
[18] Silversmit G, Depla D, Poelman H, Marin G B and De Gryse R 2004 Determination of the V2p XPS binding energies for different vanadium oxidation states (V5+ to V0+) *J. Electron Spectrosc. Relat. Phenom.* **135** 167–75
[19] Sánchez N A, Rincon C, Zambrano G, Galindo H and Prieto P 2000 Characterization of diamond-like carbon (DLC) thin films prepared by rf magnetron sputtering *Thin Solid Films* **373** 247–50
[20] Peckus D, Meškinis Š, Vasiliauskas A, Rajackaitė E, Andrulevičius M, Kopustinskas V and Tamulevičius S 2020 Structure and optical properties of diamond like carbon films containing aluminium and alumina *Appl. Surf. Sci.* **529** 147040
[21] Feng X and Xia Y 2012 Tribological properties of Ti-doped DLC coatings under ionic liquids lubricated conditions *Appl. Surf. Sci.* **258** 2433–8
[22] Lai L F, Xu Z Y and Xu J Effect of sputtering conditions on transmittance and wear resistance of diamond-like carbon film *IOP Conf. Ser.: Mater. Sci. Eng* 012008
[23] Zhao D, Mei H, Ding J C, Cheng Y, Zhang L, Zhang T F, Kwang H K and Zheng J 2023 Microstructure and properties of Mo doped DLC nanocomposite films deposited by a hybrid sputtering system *Vacuum* **208** 111732
[24] Zhairabany H, Khaksar H, Vanags E, Smits K, Sarakovskis A and Marcinauskas L 2025 Structural, mechanical, and tribological properties of molybdenum-doped diamond-like carbon films *Crystals* **15** 463
[25] Schneider J, Ulrich S, Patscheider J and Stueber M 2022 Wear study of a magnetron-sputtered TiC/aC nanocomposite coating under media-lubricated oscillating sliding conditions *Coatings* **12** 446
[26] Casiraghi C, Piazza F, Ferrari A C, Grambole D and Robertson J 2005 Bonding in hydrogenated diamond-like carbon by Raman spectroscopy *Diam. Relat. Mater.* **14** 1098–102
[27] Su Y, Huang W, Wang J, Gong X, Zhang T, Hu R, Yu W, Ruan H and Ma Y 2023 Binary elements (Si, Mo) co-doping strategy enhanced the tribological performance of diamond-like carbon films *Surf. Coat. Technol.* **471** 129905
[28] Ferrari A C and Robertson J 2001 Resonant Raman spectroscopy of disordered, amorphous, and diamondlike carbon *Phys. Rev. B* **64** 075414
[29] Zhairabany H, Khaksar H, Vanags E and Marcinauskas L 2024 Effect of molybdenum concentration and deposition temperature on the structure and tribological properties of the diamond-like carbon films *Crystals* **14** 962

[30] Zhigalina O M, Khmelenin D N, Pimenov S M, Shupegin M L, Dyachkova I G and Asadchikov V E 2018 Structure of diamond-like silicon–carbon films alloyed by vanadium *Crystallogr. Rep.* **63** 796–801
[31] Caessa J, Vuchkov T, Yaqub T B and Cavaleiro A 2021 On the microstructural, mechanical and tribological properties of Mo-Se-C coatings and their potential for friction reduction against rubber *Materials* **14** 1336
[32] Asadchikov V E *et al* 2019 Comparison of transmission electron microscopy and x-ray reflectometry data in the study of the structure of silicon-carbon nanocomposite films *Crystallogr. Rep.* **64** 793–7
[33] Vinogradov A N, Dyachkova I G, Mamontov A V, Monakhov I S, Shahbazov S Y and Shupegin M L 2020 Mechanical properties of diamond-like silicon–carbon films doped with vanadium *Crystallogr. Rep.* **65** 1002–7
[34] Komlenok M S, Arutyunyan N R, Freitag C, Zavedeev E V, Barinov A D, Shupegin M L and Pimenov S M 2021 Effect of tungsten doping on laser ablation and graphitization of diamond-like nanocomposite films *Opt. Laser Technol.* **135** 106683
[35] Pimenov S M, Zavedeev E V, Arutyunyan N R, Zilova O S, Barinov A D, Presniakov M Y and Shupegin M L 2020 Effects of titanium doping on the structure and mechanical properties of diamond-like nanocomposite films *Surf. Coat. Technol.* **402** 126300